Catalytic activity of MOF(2Fe/Co)/carbon aerogel for improving H_2O_2 and •OH generation in solar photo–electro–Fenton process

Hongying Zhao, Ying Chen, Qiusheng Peng, Qingning Wang, Guohua Zhao*

School of Chemical Science and Engineering, and Shanghai Key Lab of Chemical Assessment and Sustainability, Tongji University, 1239 Siping Road, Shanghai, 200092, China

ABSTRACT

A novel bifunctional MOF(2Fe/Co)/CA cathode with a high surface possessing area, and good electrocatalytic and photocatalytic activity, was proposed for the solar photo–electro–Fenton (SPEF) process. The optimal nFe: nCo ratio was 2:1 for successfully introducing MOF(2Fe/Co) on the surface of CA, which is due to the specific interaction affinity of FeOOH between MOF(2Fe/Co) and CA. Continuous on–site generation of H_2O_2 through an oxygen reduction reaction (ORR) was achieved over the CA cathode. The electron transfer number (n) of the ORR with CA was 2.5 in the selected potential range. Moreover, the addition of MOF can behave as the active sites for enhancing the ORR activity and hence can increase the yield of the H_2O_2. Simultaneously, the photoinduced electron (e_{cb}^-) of MOF(2Fe/Co) efficiently in–situ decomposed H_2O_2 to form hydroxyl radicals (•OH). The observation indicated that the e_{cb}^- is an efficient and new Fenton–like catalysts that is pH–independent. Efficient photo–electro–catalytic performance was exhibited when applied to degrade Rhodamine B (RhB) and dimethyl phthalate (DMP). Almost 100% RhB removal and 85% DMP removal were reached in 45 min and 120 min, respectively. The MOF(Fe/Co)/CA presented very low iron and cobalt leaching (<0.5 ppm) even in an acidic media, and it retained an efficient degradation efficiency in the wide pH range of 3–9.

© 2016 Published by Elsevier B.V.

1. Introduction

Electrochemical advanced oxidation processes (EAOP) are new attractive techniques for the disposal of the increasing amount of toxic and persistent compounds found in many types of effluents [1]. Among these processes, the electro–Fenton (EF), based on in situ production of highly reactive hydroxyl radicals, has received tremendous attention in recent years [2–4]. Compared to the classical Fenton's system, the EF process represents several advantages such as (i) the in–site continuous electrogeneration of H_2O_2, (ii) a fast degradation rate and short reaction time, and (iii) sustained Fe^{2+} regeneration through cathodic reduction. However, the Fe^{2+} in the traditional EF process is water-soluble and is unable to avoid the limitation of a homogeneous Fenton reaction especially for requiring an optimum pH $\leq$ 3 [5]. The degradation efficiency with the homogeneous EF process would be dramatically decreased with an increasing pH. Moreover, the use of Fe^{2+} may easily cause secondary metal contamination. Thus, the design and fabrication of an efficient heterogeneous EF cathode that works with a wide pH

range is the key or the purification of actual wastewater, which always has variable pH values.

Metal–organic frameworks (MOFs) are a fascinating class of high surface area and crystalline porous materials [6], They have great potential for use in applications such as in heterogeneous catalysis, gas storage, adsorption and separation, and drug delivery [7,8]. Presently, extensive studies have been carried out on the effluent purification with virgin or modified MOFs [9,10]. Previous studies indicated that iron–based MOFs can be considered as heterogeneous Fenton–like catalysts, even though they only possess Fe^{III} sites with weak Fenton activity and contain low iron concentration [11].

In addition to the Fenton-like activity, MOFs have been successfully exploited for electrocatalysis studies [12,13], such as oxygen evolution reaction (OER) and oxygen reduction reaction (ORR). The aforementioned EF reactions highlight that the formation of H_2O_2 via ORR plays a decisive role in the oxidation reaction. To improve the ORR activity, various carbonaceous cathode materials have been widely investigated, including activated carbon, graphite felt, carbon sponge and gas–diffusion electrodes. Carbon aerogel (CA), a novel porous electrode, possesses a three–dimensional (3D) network structure, high surface area and good electrical conductivity. Additionally, in our previous study, CA was widely used as

* Corresponding author.
E-mail address: g.zhao@tongji.edu.cn (G. Zhao).

an EF cathode and produced a high yield of H_2O_2 [14,15] both in acidic and neutral media. In general, the electrochemical synthesis of H_2O_2 in alkaline media has been widely reported [16], however it is more promising for H_2O_2 generation in acidic media for many applications [17], such as Fenton reaction. The ORR in acidic environment with CA cathode has not been reported in the literatures. Additionally, it is worth noting that whether the addition of electrocatalyst MOFs would increase the ORR activity.

Moreover, it has been recently reported that some MOFs exhibit excellent photocatalytic ability for wastewater treatment through which an efficient utilization of solar energy can be achieved by modifying the metal ions and organic linkers [18,19]. More significantly, the photoinduced electron of MOFs as photocathode can also interact with H_2O_2 to generate •OH $(e^- + H_2O_2 \rightarrow {}^\bullet OH + OH^-)$. This can be ascribed to one type of Fenton–like reaction, which is pH–independent in case of sufficient H_2O_2. However, few studies have focused on the photogenerated electron induced Fenton–like reaction.

Inspired by the above idea, we fabricated mixed metal ion MOF(2Fe/Co)/CA cathode, which was further applied in solar photo–Fenton process for wastewater treatment. In this system, MOF(2Fe/Co) possessed bifunctional catalytic activities in terms of photocatalysis and electrocatalysis, while the CA cathode was served for H_2O_2 synthesis via the 2–electron pathway. The nFe/nCo ratio was optimized to 2:1 for successfully growing on the surface of the CA substrate. Rhodamine B (RhB) and dimethyl phthalate (DMP) with low biodegradability were selected as model target contaminates for evaluating the SPEF catalytic activity since they are representative of azo–dyes and endocrine disrupting chemicals moderns, respectively. The main purpose of this work is (1) to explore efficient heterogeneous EF process for effluent purification in wide pH range, (2) to investigate the effect of MOF(2Fe/Co) on the H_2O_2 generation via 2–electron pathway of ORR over CA cathode, and (3) to elucidate catalytic activity of photogenerated electron (e_{cb}^-) as Fenton-like catalyst, which is theoretically regardless of operation pH value. In addition, a plausible enhanced reaction mechanism in SPEF oxidation of organic pollutants is proposed.

2. Experimental

2.1. Reagents and materials

Analytically pure iron nitrate ($Fe(NO_3)_3 \cdot 9H_2O$), cobalt chloride ($CoCl_2 \cdot 6H_2O$), hydrofluoric acid (HF, ≥40 wt%), Ethyl alcohol, methanol, isopropanol, and sodium sulfate were purchased from Sinopharm (Shanghai, China). Resorcinol, formaldehyde, sodium carbonate, acetone, sodium hydroxide, trimesic acid (H_3BTC), rhodamine B, and dimethyl phthalate were obtained from Aladdin Co., China. 5,5–dimethylpyrroline–1–oxide (DMPO) was obtained from Sigma–Aldrich. All of the chemicals were analytical grade and used without further purification except that methanol is chromatographic grade. All solutions were prepared with deionized water.

2.2. Preparation of MOF(2Fe/Co)/CA cathode

Synthesis of MOF(Fe/Co) catalysts with different nFe: nCo ratio was conducted [13]. The total amount of $Fe(NO_3)_3 \cdot 9H_2O$ and $CoCl_2 \cdot 6H_2O$ was controlled at 7.5 mmol. The theoretical amount of $Fe(NO_3)_3 \cdot 9H_2O$ and $CoCl_2 \cdot 6H_2O$ for different MOF(Fe/Co) combinations was calculated according to the nFe: nCo ratio of 1:1, 2:1 and 3:1. For MOF(2Fe/Co) with nFe:nCo = 2:1, 5 mmol $Fe(NO_3)_3 \cdot 9H_2O$, 2.5 mmol $CoCl_2 \cdot 6H_2O$, 4.95 mmol H_3BTC and 3 mmol HF was added to 35 mL water under constant magnetic stirring at room temperature. After stirring for 1 h, the mixture solution was transferred to a Teflon–lined stainless autoclave and sealed, which was then

placed in an oven at 160 °C for three days. After the hydrothermal reaction, the obtained product was firstly respectively treated with water and then ethanol for 6 h to remove the residual organic ligand, then dried in vacuum oven at 60 °C for 2 h. The MOF(Fe/Co) and MOF(3Fe/Co) were prepared according to the same procedures except with different theoretical amount of $Fe(NO_3)_3 \cdot 9H_2O$ and $CoCl_2 \cdot 6H_2O$.

The synthesis of MOF(2Fe/Co)/CA cathode was conducted. Firstly, the carbon aerogels (CA) electrode was prepared based on our previous work [20,21]. The bifunctional MOF(Fe/Co)/CA cathode was prepared with the same procedures that were mentioned above, except that the obtained CA was placed into an autocalve and fixed in vertical direction once the mixture precursor solution was transfered into autoclave.

2.3. Characterization methods

The X–ray diffraction (XRD) measurements were collected on a Rigaku–D/max2550 powder diffractometer with Cu Kα radiation (40 kV, 30 mA over the 2Θ range, 3–80 °C). The morphology and microstructure were characterized by scanning electron microscopy (SEM, Hitachi–S4800). Elemental analysis was performed by inductively coupled plasma–atomic emission spectrometry (ICP–AES, PE OPTIMA 2100DV). Raman spectra were obtained on a Raman spectrometer (Renishaw Crop., UK) using a He/Ne laser with the wavelength of 515 nm. Electron spin resonance (ESR) spectra were obtained on a Bruker EMX Xplus–10/12 with a Microwave Bridge (microwave frequency, 9.853 GHz; microwave power, 20 mW; modulation amplitude, 1 G; modulation frequency, 100 kHz). For electron paramagnetic resonance (EPR) measurements, 50 μL of the sample was collected from the suspension EF system and mixed with 5,5–dimethypylpyrroline–1–oxide (DMPO) to create DMPO–•OH adducts (Bruker, EMX plus–10/12).

2.4. Electrochemical property test

The ORR was examined using a Pine AFMSRXE 1523. First, 10 mg of MOF(2Fe/Co)/CA and CA were added into a mixture of 2.25 mL of water and a 250 μL Nafion solution (5 wt.%, Alfar Aesar). Ultrasonic oscillation was applied for 60 min to yield a homogenous suspension ink. A 20–μL ink aliquot was dropped onto a glassy carbon disk electrode (geometric area of 0.1963 cm^2) for the RDE test. Both working electrodes were eventually obtained after drying overnight at room temperature. The electrochemical measurements of the working electrodes containing the catalysts were carried out on a computer–controlled CHI 660D electrochemical station (Chenhua Instrument Co. Ltd., China) using traditional three–electrode system in 50 mM Na_2SO_4 solution at pH = 3 which was adjusted with 100 mM of H_2SO_4. A KCl–saturated Hg/Hg_2Cl_2 electrode and a platinum wire were used as the reference electrode and the counter electrode, respectively.

Before all electrochemical measurements were taken, CVs were recorded in N_2–saturated 50 mM Na_2SO_4 solution with pH = 3 in the corresponding potential ranges at a sweep rate of 1 mV s^{-1} to obtain a stable electrochemical profile. For each RDE test, LSV was performed in N_2–saturated Na_2SO_4 solution at 0.2 V to −1.0 V at a sweep rate of 1 mV s^{-1} and then performed in O_2–saturated Na_2SO_4 solution under the same operational conditions. The differences in LSV–derived current density in O_2–saturated electrolyte and in N_2–saturated electrolyte at a sweep rate of 1 mV s^{-1} are regarded as the ORR current density of the catalysts.

2.5. Degradation experiment and analysis

The solar photo–electro–Fenton oxidation of organic pollutants (RhB and DMP) was carried out in a cylindrical single compart-

ment cell equipped with an Air–blowing device and a jacketed cooler to retain a constant temperature. The light source was a 500 W Xe lamp. A 100 mL 50 ppm RhB or DMP in Na_2SO_4 (0.1 M) solution served as the simulated wastewater. The MOF(2Fe/Co)/CA and CA electrodes (working area of 3 cm^2) worked as the cathode, and a BDD acted as the anode with the same area, while the distance between the two electrodes was 2 cm. Air was fed onto the cathode surface at a flow rate of 300 mL min^{-1}. The Pt foil acted as the counter electrode and a saturated calomel electrode (SCE) acted as the reference electrode. Degradation samples were taken at set intervals using a 5–mL syringe and centrifuged at 10,000 rpm for 5 min. The supernatant was immediately filtered through a 0.22–μm filter film. The reusability of the MOF(2Fe/Co)/CA electrodes was evaluated by collecting the used electrodes, washing them with deionized water, drying them under vacuum, and using them for an additional reaction under similar experimental conditions.

The RhB concentration during the reaction was analyzed by a UV–vis spectrophotometer (Agilent, 8453) at a maximum absorbance wavelength for RhB of 554 nm. The DMP concentration during the degradation was measured by high–performance liquid chromatography (HPLC, Agilent HP1100) equipped with a reverse phase AQ–C18 column (4.6 mm × 250 mm, particles size 5 μm) and a UV detector. The detection wavelength was set at 270 nm, and the mobile phase was a mixed solution of 30% methanol and 70% water (V/V). For each UV–vis and HPLC analysis, 1–2 mL RhB solution was taken up in fixed interval and then added with excess isopropyl alcohol for quenching the residual Fenton reaction. The intermediates of DMP were detected by GC–MS, which was carried out on an Agilent 6890GC/5973MSD with a capillary column (Agilent DB–5MS, 30 m × 0.25 mm, 0.25 μm). A sample for GC–MS analysis was prepared as follows: after 5 min reaction time, 5 mL sample was taken and filtered with a filter of 0.22 μm. The aqueous sample was freeze–dried, then the residues were trimethylsilylated with 0.2 mL of anhydrous pyridine, 0.1 mL of hexamethyldisilazane, and 0.05 mL of chlorotrimethylsilane at room temperature. Finally the samples were dehydrated using muffled Na_2SO_4 and concentrated to 0.5 mL for GC–MS analysis. Correspondingly, the GC oven temperature program for the sample was: 323.15 K hold 5 min, rate 10 K/min to 373.15 K, hold for 3 min, rate 30 K/min to 673.15 K, hold for 4 min. The injector temperature was 280 °C and helium was employed as carrier gas.

The total organic carbon (TOC) concentration was determined using a TOC analyzer (multi N/C 3100 TOC/TN analyzer, Analytikjena, Germany). For each TOC analysis, 15 mL RhB solution after the SPEF oxidation 60 min was immediately treated with scavenging reagent (0.1 M Na_2SO_3, 0.1 M KH_2PO_4, 0.1 M KI and 0.05 M NaOH) to obtain accurate TOC values [22,23]. This procedure led to a complete reduction of the residual H_2O_2 as well as to the removal of most of the iron. The total iron and copper leaching concentrations were determined by elemental analysis using ICP–AES (PE OPTIMA 2100DV). The determination of H_2O_2 was performed by using titanium oxysulfate as indicator and UV–vis spectrophotometer (Agilent 8453, Agilent Corporation, U.S.) was used to measure the absorbance of the complex compound solution at the maximum absorption wavelength λ = 409 nm [14].

3. Results and discussion

3.1. The fabrication, structural and surface properties of the bifunctional MOF(2Fe/Co)/CA cathode

The MOF(2Fe/Co)/CA cathode was fabricated by a modified hydrothermal reaction. The MOF(Fe/Co) catalysts, with different nFe/nCo ratios of 1:1, 2:1 and 3:1, were successfully obtained.

Nevertheless, only when the nFe/nCo was 2:1, the MOF(2Fe/Co) can successfully grow on the surface of CA. In order to investigate the interaction between CA and MOF(2Fe/Co), the composition and crystallographic structure of MOF(2Fe/Co)/CA cathode and MOF(Fe/Co) catalysts with different nFe/nCo ratio were examined by XRD. As exhibited in Fig. 1, all samples possessed the main diffraction peaks (2θ = 6.2°, 10.2°, 11.0°, 11.9°, 20.1°, 24.1°, 27.6°, 28.1°, 32.8°, 33.4° and 36.5°) of crystal MOF(Fe/Co) as previously reported in the literature [24]. Note that for MOF(2Fe/Co)/CA electrode, the new peaks (2θ = 16.7°, 26.8°, 43.2°, 46.6°, 50.2°, 56°, 62.6°, 64.7°, 68°, 71.5° and 73.3°) characteristic of goethite (FeOOH) appeared, indicating the specific interaction affinity of FeOOH between MOF(2Fe/Co) and CA. With an nFe/nCo ratio of 2:1, part of ferric ions were formed ferric hydroxide at the surface of CA, and then transformed to FeOOH upon drying.

To further elucidate the formation of special surface interaction between substrate CA and MOF (2Fe/Co), the additional in–depth studies with Raman and IR were carried out. As presented in Fig. 2, typical Raman spectra in high frequency region due to organic part of MOF framework were obtained for MOF(2Fe/Co) [11,25]. The bands at 1604 and 1002 cm^{-1} were due to the ν(C=C) modes of the benzene ring; the peak at 1537 and 1474 cm^{-1} were assigned to the –(C=O)O– group, while the band at 1372 and 1230 cm^{-1} were ascribed to –(C=O)OH group; the bands at 810 and 727 cm^{-1} were associated with C—H vibration. In the low frequency region, the band at 660, 494, 396, 298, 216, 168 cm^{-1} were possibly characteristic of vibrational modes directly involving Fe(III) and Co(II) species in MOF catalyst. After introducing MOF(2Fe/Co) to the surface of CA, the high frequency modes of organic portion of framework disappeared, possibly being overlapped by the two strong bands of
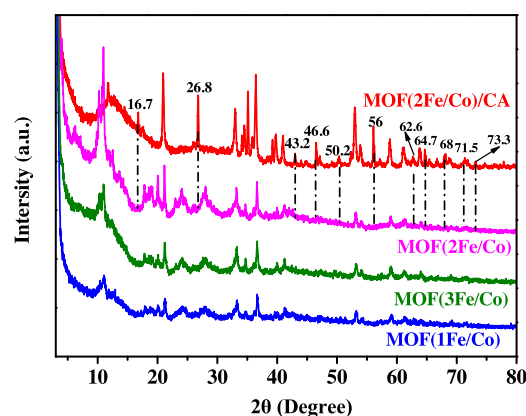

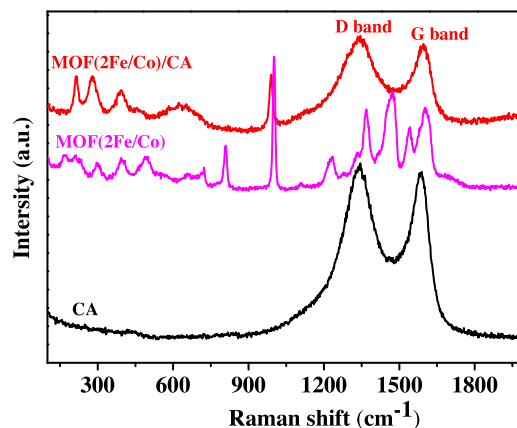**Fig. 1.** The XRD patterns of MOF(2Fe/Co)/CA and CA electrodes.

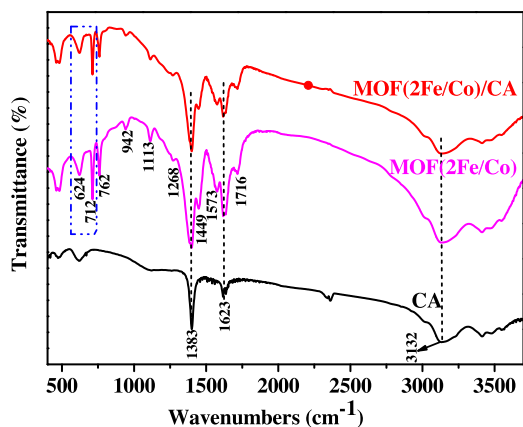**Fig. 2.** The Raman spectra of MOF(2Fe/Co)/CA and CA electrodes.

Fig. 3. The FTIR spectra of MOF(2Fe/Co)/CA and CA electrodes.

carbon. The bands located at ∼1341 cm^{-1} were corresponded to the disorder–induced band of the graphitic carbon (D band), while those at 1589 and 1596 cm^{-1} were due to the bond stretching of all pairs of the sp^2 carbon (G band). Moreover, the new peaks at 215, 280 and 393 cm^{-1} were assigned to FeOOH, confirming the new generation of FeOOH on MOF(2Fe/Co)/CA cathode. Moreover, the spectra of CA and MOF(2Fe/Co)/CA electrodes exhibited typical behavior for carbon material. The red shift (∼7 cm^{-1}) of G band for MOF(2Fe/Co)/CA most likely results from the increased disorder degree [26,27]. The I$_D$/I$_G$ ratio are 1.05 and 1.11 for CA and MOF(2Fe/Co)/CA, respectively. The I$_D$/I$_G$ ratio >1 indicates a relative high degree of disorder in graphitic phase [26,27].

Fig. 3 exhibits the FTIR patterns of MOF(2Fe/Co), MOF(2Fe/Co)/CA and CA. The two bands at 3132, 1383 and 1623 cm^{-1} attributed to hydrogen bonded O—H groups, –(C=O)OH groups and H—O—H groups respectively were observed for all the samples. The peak at 1623 cm^{-1} is also assigned to ν(C—O) bond of carboxylate groups especially for MOF(2Fe/Co), MOF(2Fe/Co)/CA samples. The absence of other two sharp peaks near 762 and 712 cm^{-1} corresponds to C—H bending vibrations of benzene. Note that, compared to the MOF(2Fe/Co), the intensity of all peaks in MOF(2Fe/Co)/CA decreased except the peak at 624 cm^{-1}. The I$_{624}$/I$_{712}$ (I$_{624}$: the intensity of peak at 624 cm^{-1}; I$_{712}$: the intensity of peak at 712 cm^{-1}) for MOF(2Fe/Co) is 0.39, which was increased to 0.46 for MOF(2Fe/Co)/CA. The adsorption band at 624 cm^{-1} can also be characteristic of the Fe–O stretching vibration in the FeOOH. All the observation suggested the new generation of FeOOH in MOF(2Fe/Co)/CA cathode, which is agreement with Raman and XRD results as we discussed above.

The morphologies of MOF(2Fe/Co)/CA and pure CA electrodes were examined through SEM, as presented in Fig. 4A and B. MOF(2Fe/Co) with rectangular shape successfully grew on the surface of CA. Additionally, the surface iron and cobalt on MOF(2Fe/Co)/CA electrode were confirmed by EDS analysis (Fig. 4C). The EDS elementary mapping further revealed that all the iron and cobalt species were uniformly dispersed on the electrode surface.

3.2. Efficient degradation of organic pollutants with MOF(2Fe/Co)/CA cathode in SPEF oxidation process

In order to explore the catalytic oxidation ability of heterogeneous SPEF process with MOF(2Fe/Co)/CA cathode for wastewater treatment, the degradation efficiency were evaluated by rhodamine B (RhB) and dimethyl phthalate (DMP) at pH 3 with the initial concentration of 20 mg L^{-1}. The RhB removal in different processes such as solar photo (SP), electro–Fenton (EF), solar

Table 1
Main detected intermediates by GC–MS during DMP degradation in SPEF process with MOF(2Fe/Co)/CA.

Retention (min)	Product	Molecluar structure
2.204	2–methyl–1–propano	
9.479	Lactic acid	
9.560	Oxalic acid	
11.790	Benzoic acid	
13.035	Dimethyl phthalate	
13.251	Adapic Acid	
13.419	Phenol	
14.106	Terephthalic acid	
16.504	1,4–Benzenediol	

photo–electro–Fenton (SPEF) are shown in Fig. 5A. In solo SP process, only 2% RhB was removed. For pure CA, an approximately 16% RhB removal at 75 min was obtained in ES process due to the electrosorption capability of porous CA. While in SPEF process, RhB removal with CA was slightly increased to 22%, attributed to the •OH radicals formed through decomposing H$_2$O$_2$ under solar light irradiation. Note that, no matter with which process (EF or SPEF) was utilized, the RhB removal efficiency was greatly enhanced over that of novel MOF(2Fe/Co)/CA cathode. For example, almost 100% and 48% RhB was removed after only 45 min in SPEF and EF process, respectively. It is interesting to find that, with the introduction of solar light irradiation on cathode, the RhB degradation efficiency was increased by 108%. This observation obviously indicates that the photoinduced electrons (e$_{cb}^-$) of MOF(2Fe/Co) can react with H$_2$O$_2$ for improving the •OH generation. The DMP degradation efficiency with CA and MOF(2Fe/Co)/CA in various processes followed the same tendency as RhB removal, which was exhibited in Fig. 5B. At 120 min, 85% DMP removal can be reached in
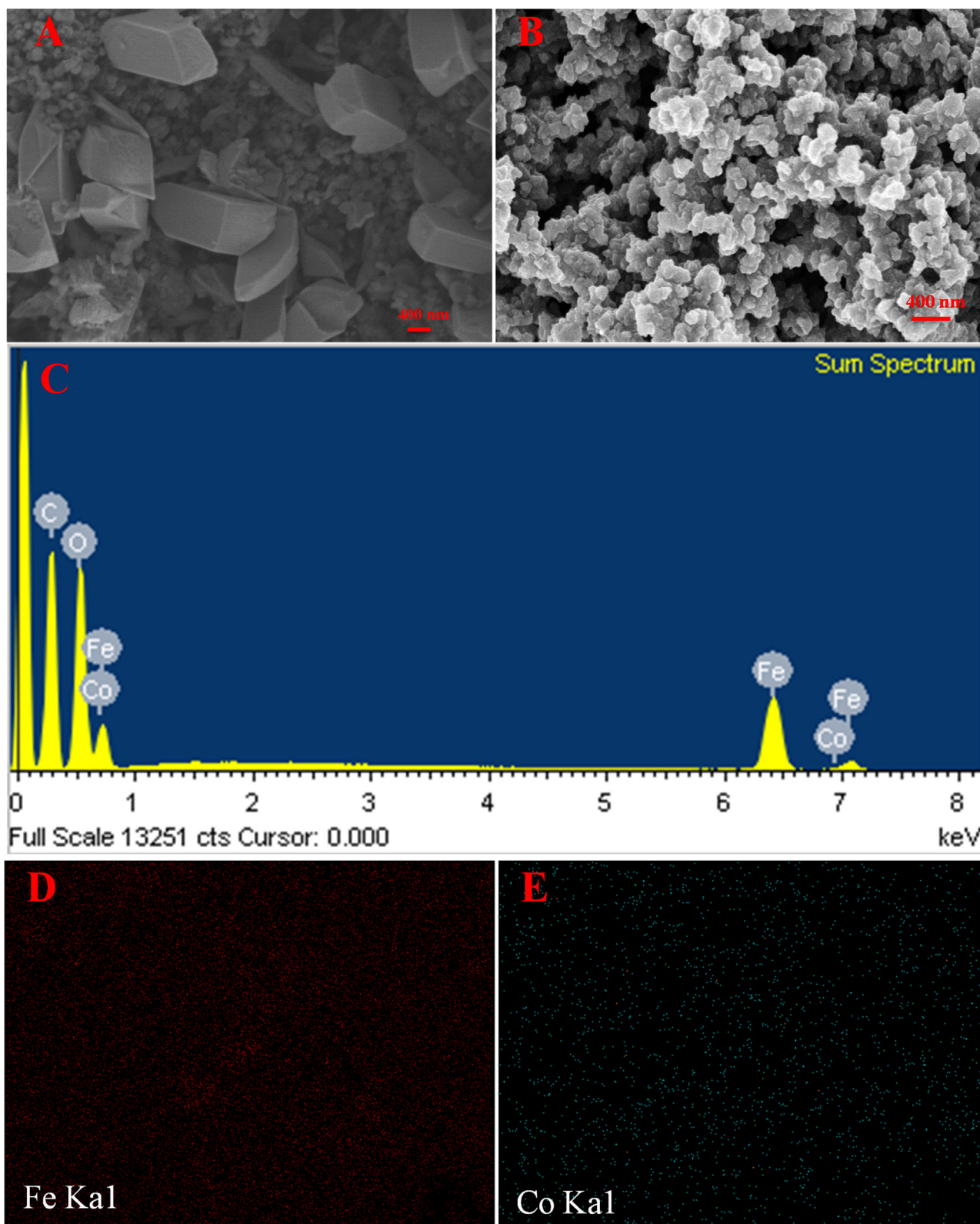
Fig. 4. The SEM images of the prepared MOF(2Fe/Co)/CA electrode (A) and pure CA (B). EDS spectra (C) and EDS elemental mappings of MOF(2Fe/Co)/CA electrode.

SPEF process, suggesting again that this fabricated MOF(2Fe/Co)/CA is an promising cathode in SPEF system for efficiently removing various organic pollutants.

Considering that DMP is potential endocrine disrupter, its existence in environmental has raised great concerns. The process of DMP degradation was further analyzed with GC–MS to identify the aromatic carboxylic acids as by-products during the SPEF process with MOF(2Fe/Co)/CA photocathode. The main intermediates produced at 5 and 20 min were summarized in Table 1 . Based on the identified intermediates and literature work, the pro-
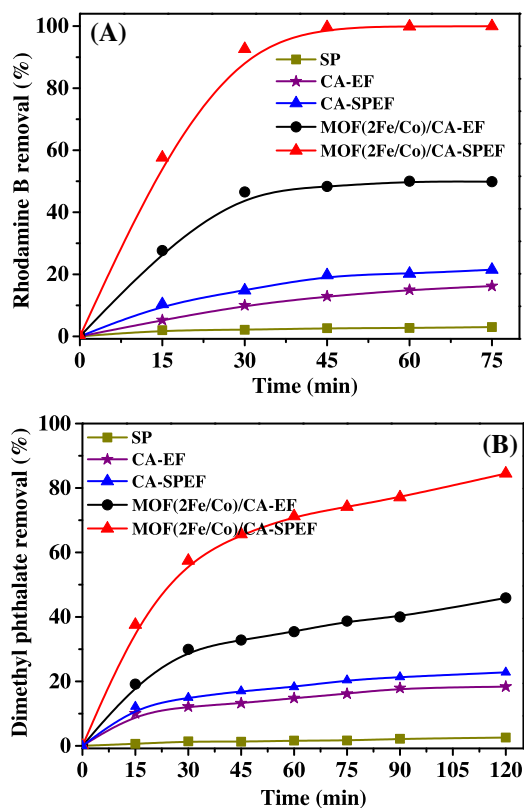
Fig. 5. The removal efficiency of Rhodamine B (A) and dimethyl phthalate (B) in different process at pH = 3.

Fig. 6. Proposed degradation pathway of aqueous DMP in SPEF process with MOF(2Fe/Co)/CA cathode.

posed degradation pathways A–C were shown in Fig. 6. In route A, phthalic anhydride (compound 3) was formed through loss of methoxyl groups, abstraction of protons, and remove of methanol [28–30]. Decarboxylation from compound 3 resulted in phenol (compound 6). Routes B–C were initiated by •OH attacking the terephthalic acid (compound 2). The attack of •OH to the aromatic ring of compound 2 led to the formation of two hydroxylated intermediates (compound 4 and 5). The phenyl ring of compound 4 was opened into adapic acid (compound 7). Simultaneously, cleavage of alkyl–oxygen bond of compound 4 generated benzoic acid (compound 8). Route D involved the further oxidation of compound 2 into p–hydroxylbenzoic acid (compound 5), which is further oxidized into 1,4–benzenediol (compound 9) [31]. The generated intermediates (compound 6–9) were further decomposed to carboxylic acids. Ultimately, the mineralization of DMP was completely accomplished until almost all of formed carboxylic acids decompose to CO_2 and H_2O.

As is known, the mineralization rate is much lower than the degradation rate and the mineralization degree, to some extent, represents catalytic efficiency for the disposal of actual wastewater. As example, the total organic carbon (TOC) of RhB solution catalyzed by MOF(2Fe/Co)/CA was measured as an indicator for the organic mineralization at different time intervals (see Fig. 7). The TOC removal was increased with increasing the reaction time, mostly due to the further decomposition of formed intermediates. The TOC removal of RhB after 10 h in EF process was 61%, implying Fenton–like oxidation catalytic performance of MOF(2Fe/Co) is not very high. This was possibly due to the limited Fenton catalytic sites (Fe^{III}) in MOF(2Fe/Co) catalyst, which is in agreement with our previous observation [11]. Nevertheless, by introducing solar light irradiation, the TOC removal efficiency of RhB was greatly increased. In SPEF process, at 10 h, the TOC removal of RhB was 91%, which is 1.5 times higher than that in EF system.
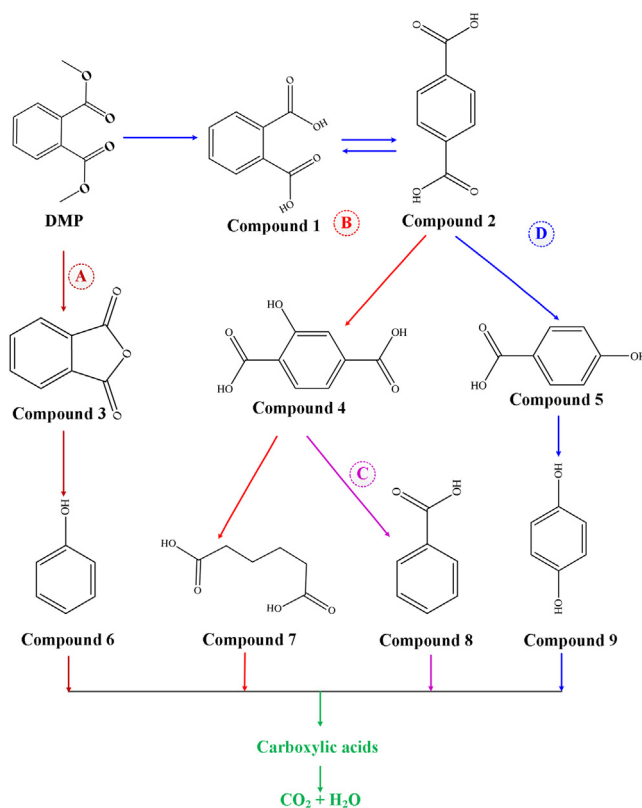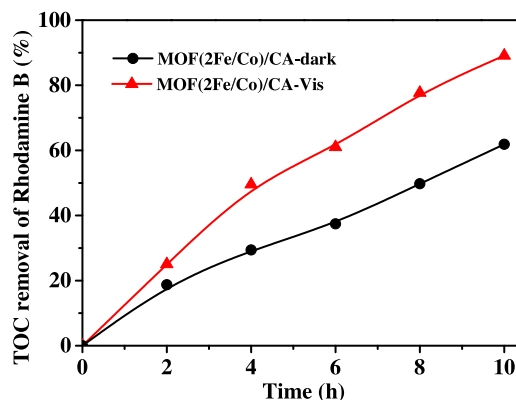

Fig. 7. The TOC removal of Rhodamine B with MOF(2Fe/Co)/CA cathode in SPEF and EF process.

3.3. The improved electrocatalytic and photocatalytic properties of MOF(2Fe/Co)/CA respectively for the generation of H_2O_2 and •OH radicals

The in–situ electrochemical production of H_2O_2 via oxygen reduction reaction (ORR) plays a decisive role in EF technology and is affected by the properties of cathode materials and reaction potential. As exhibited in Fig. 8, after introducing MOF(2Fe/Co) into CA, the H_2O_2 production was increased at the bias potential between −0.3 and −0.9 V (vs. SCE). Once the bias potential is more negative than −1.1 V (vs. SCE), the H_2O_2 generation with MOF(2Fe/Co)/CA decreased, which was smaller than CA cathode. This is because the two–electron reduction of O_2 was suppressed by side reactions when the applied potential became more negative, such as H_2 evolution reaction, one–electron and/or four–electron
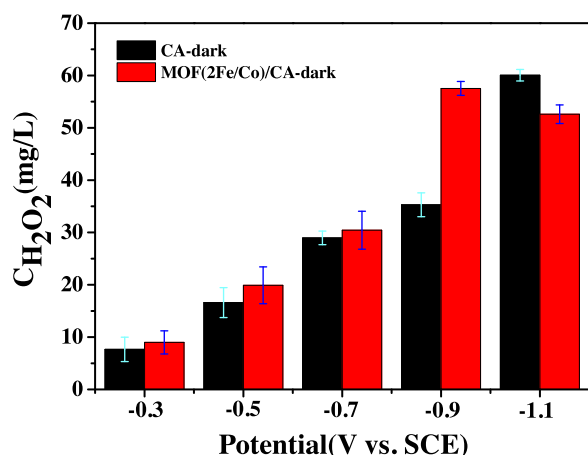
Fig. 8. The effect of potential on the cathodic generation of H_2O_2 over MOF(2Fe/Co)/CA cathode at pH = 3.
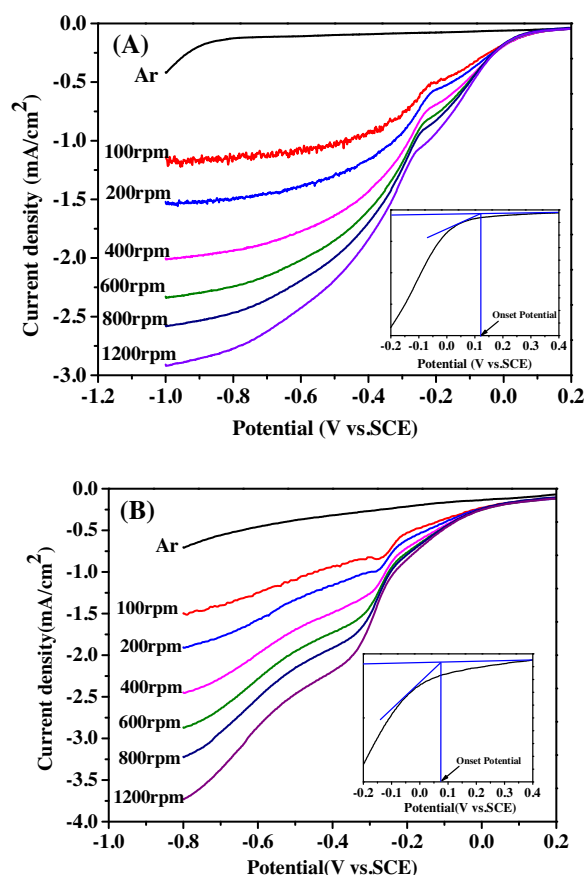

Fig. 9. Linear–sweep voltammograms of (A) MOF(2Fe/Co)CA and (B) CA catalyst measured on a rotating disk electrode at different rotating speeds with pH 3 (scan rate 5 mV/s).

reduction of O_2. That is why we carried out the degradation experiment at bias potential of −0.9 V to obtain the highest H_2O_2 yield.

To gain further (Fig. 9) insight into the ORR catalytic mechanism over modified MOF(2Fe/Co)/CA and CA cathodes, rotating disk measurements were recorded in 0.05 M Na_2SO_4 solution under O_2 atmosphere. The acidic medium is not only a more promising condition for electrochemical synthesis of H_2O_2, but also is often desired for Fenton–based technologies that using H_2O_2. Thus, the pH of reaction solution was adjusted to 3 with dilute H_2SO_4 in this work. Fig. 9 presents the ORR activities of these two cathodes at differ-
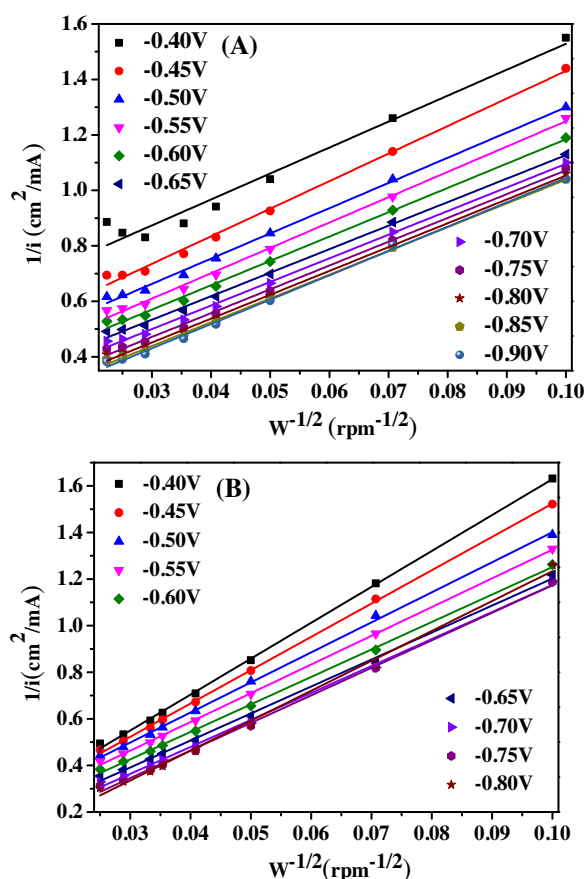

Fig. 10. The Koutecky–Levich curves of the (A) MOF(2Fe/Co)/CA and (B) CA catalysts at various potentials.

ent rotation speeds. The ORR onset potential is 0.054 V (vs. SCE) for CA. However, MOF(2Fe/Co)/CA cathode exhibited an improved ORR activity with more positive onset potential of 0.125 V (vs. SCE). Additionally, the H_2 evolution reaction on CA and MOF(2Fe/Co)/CA emerged when the potential was more negative than −0.8 and −0.9 V (vs. SCE), respectively. All of these results suggested that the ORR activity of CA cathode was improved after doping with MOF(2Fe/Co).

The number of transferred electron (n) in the ORR over the investigated catalyst was calculated according to the Koutecky–Levich (K–L) equations (Eqs. (1) and (2)):

$$\frac{1}{j} = \frac{1}{j_k} + \frac{1}{j_D} = \frac{1}{j_k} + \frac{1}{B \bullet \sqrt{\omega}} \tag{1}$$

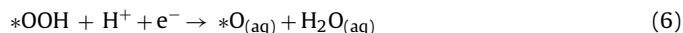$$B = 0.2nFD_{O_2}{}^{2/3}\nu^{-1/6}C_{O_2} = A \times n \tag{2}$$

Where j is the measured current density, which is related to the kinetic current density (j_K) and the diffusion–limited current density (j_D), and ω is the angular velocity of the rotating disc electrode. Where F is the Faraday constant, C_{O2} is the bulk concentration of O_2, υ is the kinematic viscosity of the electrolyte and D_0 is the diffusion coefficient. The constant 0.2 is adopted when the rotation speed is expressed in rpm. All the parameter contributions (denoted as A) in Na_2SO_4 solution to Eq. (2) was investigated by standard Pt/C electrocatalyst (20 wt% Pt on carbon, Shanghai Macklin Biochemical Co., Ltd) with n = 3.9–4.0.

The K–L plots (Fig. 10) for the two cathodes at various potentials (from −0.4 to −0.9 V vs. SCE) presented good linearity. Note that, the intercept of K–L curves for CA was more close to zero, suggesting the oxygen diffusion was dominant in ORR process. In

general, the slope of K–L curves remains constant in given potentials; however, the parallel relationship of K–L curves is not fully obtained in this work especially for CA, indicating the combination of a two–electron and four–electron pathway. In the two–electron pathway, the oxygen can be reduced to H_2O_2 (Eq.(3)–(5)), where * denotes an unoccupied active site, and OOH* denotes the single adsorbed intermediate [32,33].

$$O_2 + H^+ + e^- + * \rightarrow *OOH \tag{3}$$

$$*OOH + H^+ + e^- \rightarrow H_2O_2 + * \tag{4}$$

$$O_2 + 2H^+ + 2e^- \rightarrow H_2O_2 \tag{5}$$
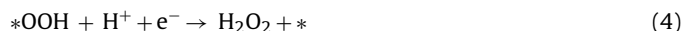
In contrast, the four–electron pathway can be described as follow (Eqs. (3) and (6)–(9))

$$O_2 + H^+ + e^- + * \rightarrow *OOH \tag{3}$$

$$*OOH + H^+ + e^- \rightarrow *O_{(aq)} + H_2O_{(aq)} \tag{6}$$

$$*O_{(aq)} + H^+ + e^- \rightarrow *OH_{(aq)} \tag{7}$$

$$*OH_{(aq)} + H^+ + e^- \rightarrow H_2O_{(aq)} + * \tag{8}$$

$$O_2 + 4H^+ + 4e^- \rightarrow 2H_2O \tag{9}$$

The electron transfer number per O_2 can be evaluated through Eq. (2) to understand the overall oxygen reduction pathway in Na_2SO_4 solution at pH 3. The parameters contribution A was calculated to be $0.032\,mC\,S^{-1/2}$ in this Na_2SO_4 solution. The electron transfer number is calculated to be 2.5 for CA in the selected potential range, implying that the ORR process on CA cathode is dominated by a two–electron pathway. With the addition of MOF(2Fe/Co) catalyst, the ORR process was gradually controlled by four–electron pathway with the electron transfer number of 3.5. The observation demonstrated that the porous CA cathode is an excellent electro–Fenton cathode with high selectivity for two–electron reduction of oxygen. The introduction of MOF(2Fe/Co) restrains the selective two–electron reduction of O_2 but promotes the whole ORR activity, which finally improves the yield of H_2O_2.

To investigate the optical adsorption property, the UV diffraction reflection spectroscopy (UV–DRS) was recorded. One adsorption band in the visible range was observed at 450–650 nm. The corresponding band gap of 1.96 eV, which was calculated from the Tauc plot (Fig. 11A, inset), can be assigned to the ligand–to–metal charge transfer [34]. Another calculated band gap of 2.75 eV can be originated from the d–d spin–allowed transition of the Co^{2+} ion [34]. Obviously, these band gaps demonstrate that photocatalysis of MOF(2Fe/Co) were visible light responsive. The Mott–Schottky plot of bi–MOF(2Fe/Co) was measured at a frequency of 2000 Hz (Fig. 11B), and the positive slope indicates a n–type semiconductor. The flat–band potential (V_{fb}) of MOF(2Fe/Co), determined from the intersection, is around −0.64 V versus SCE. In general, the conduction band position is more negative by 0.1 V than the flat–band potential for n–type semiconductors [35]. Thus, the conduction band (LUMO) of MOF(2Fe/Co) was calculated as −0.54 V versus SCE (equivalent to −0.3 V vs. NHE). According to the band gap of 1.96 V, as discussed above, the valence band (HOMO) can be calculated to 1.42 V vs. SCE (equivalent to 1.66 V vs. NHE).

The photoresponse of MOF(2Fe/Co)/CA as photocathode was further carried out respectively with continuous feeding N_2 and O_2. As shown in Fig. 12, the photocurrent density was increased once turning on the visible light was introduced. Moreover, MOF(2Fe/Co)/CA exhibited higher photocurrent density with feeding gas O_2 than with N_2, when investigating that the photoinduced electron (e_{cb}^-) can be reacted with O_2 (Eq.(11)) and/or electrogenerated H_2O_2 (Eq.(13)). The collective observation gain confirmed
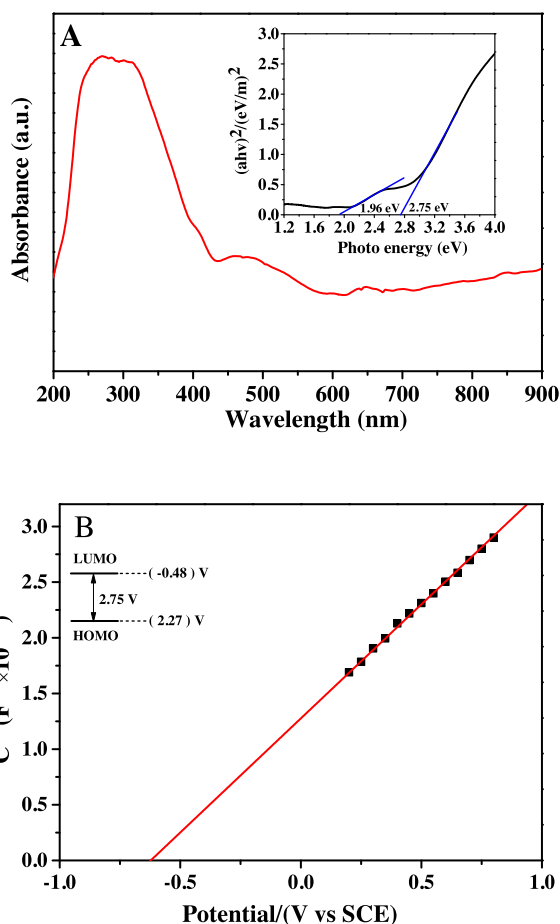

Fig. 11. The UV–DRS adsorption spectrum of MOF(2Fe/Co)/CA. Inset: corresponding Tauc plot (A); and Mott–Schottky plot of MOF(2Fe/Co)/CA (B).

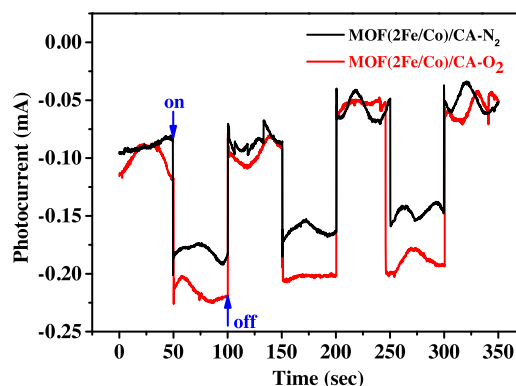**Fig. 12.** The transient photocurrent responses of MOF(2Fe/Co)/CA with feeding O_2 and N_2 in 0.1 M Na_2SO_4 aqueous solution under visible light irradiation.

that the e_{cb}^- in MOF(2Fe/Co)/CA greatly favored the decomposing H_2O_2 to generate active •OH sites.

3.4. Plausible enhanced catalytic oxidation mechanism with MOF(2Fe/Co)/CA electrode in SPEF process

It is well known that the on-site continuously generated •OH radicals are the dominant oxidants involved in the mineralization of organic pollutants in Fenton–based system. Spin–trapping EPR with 5,5–dimethypylpyrrolinr–1–oxide (DMPO) was therefore employed to compare the formation of •OH in SP, EF and SPEF processes with MOF(2Fe/Co)/CA. Moreover, the effect of $O_2^{•-}$ radicals
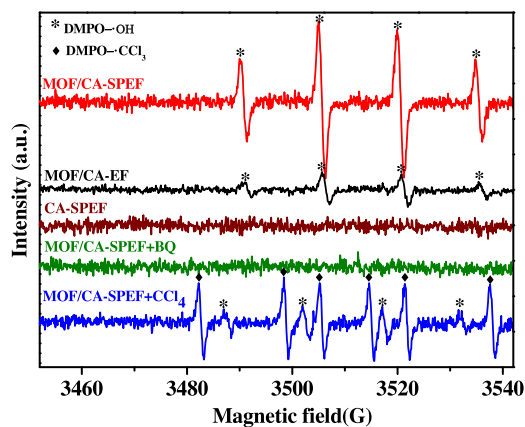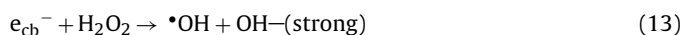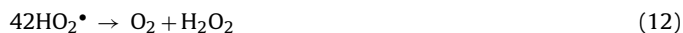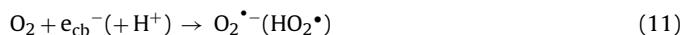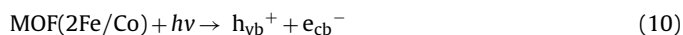
Fig. 13. DMPO spin trapping EPR spectra over CA and MOF(2Fe/Co)/CA cathode in EF and SPEF processes at initial pH 3.

Fig. 14. Degradation of RhB in the presence of different scavengers at pH 3.

and photoinduced electron (e_{cb}^-) were identified by adding different scavengers. The 1,4–benzoquinone (BQ) was used as superoxide anion ($O_2^{\bullet-}$) quencher. CCl_4 were adopted to quench photogenerated electron (e_{cb}^-). In addition to the Reactions (1)–(1), the classical mechanism of photocatalytic oxidation in SPEF has the following steps:

$$MOF(2Fe/Co) + h\nu \rightarrow h_{vb}^+ + e_{cb}^- \tag{10}$$

$$O_2 + e_{cb}^- (+ H^+) \rightarrow O_2^{\bullet-}(HO_2^\bullet) \tag{11}$$

$$42HO_2^\bullet \rightarrow O_2 + H_2O_2 \tag{12}$$

$$e_{cb}^- + H_2O_2 \rightarrow {}^\bullet OH + OH{-}(strong) \tag{13}$$

$$H_2O_2 + h\nu \rightarrow 2{}^\bullet OH(weak) \tag{14}$$

In SPEF process, the strong EPR signal with an intensity ratio of 1:2:2:1 assigned to DMPO–$^\bullet$OH was obtained for MOF(2Fe/Co)/CA cathode (see Fig. 13). The intensity of DMPO–$^\bullet$OH generated in EF process was relatively low, indicating the weak catalytic performance of MOF(2Fe/Co) for decomposing H_2O_2. For pure CA, almost no $^\bullet$OH was formed in SPEF, suggesting that the Reaction (14) is not important due to the sub–millimolar (mM) H_2O_2 concentration used [36]. Interestingly, we found that the signal of DMPO–$^\bullet$OH completely disappeared after the addition of BQ. This is due to that the key parameter in controlling the H_2O_2 generation through ORR (Eqs. (3) and (4)) and photocatalytic reaction (Eqs. (11) and (12)) is the $O_2^\bullet$–radicals. Based on the above analysis, photoinduced e_{cb}^- plays as dominant role for the formation of $^\bullet$OH through Eq. (13). In another world, this is one type Fenton–like reaction induced by electron. The introduction of CCl_4 reduced the intensity of DMPO–$\bullet$OH signal. However, CCl_4 can not only quench e_{cb}^- but also be oxidized by $^\bullet$OH to $^\bullet CCl_3$ radicals, which were then trapped by DMPO. Thus, DMPO–$^\bullet CCl_3$ adduct with a typical 6–lined spectrum as well as DMPO–$^\bullet$OH spectrum was detected. So, it is hard to determine whether the decrease of the intensity of DMPO–$^\bullet$OH was due to the quenching of e_{cb}^-.

With the aim of clarifying the contribution of each type of active sites ($^\bullet$OH, $O_2^\bullet-$, photoinduced e_{cb}^-), we further analyzed RhB removal efficiency in SPEF processes by adding the same scavengers as discussed above. Additionally, the t–butanol was used as hydroxyl radical ($^\bullet$OH) quencher. SOD, instead of 1,4–benzoquinone, was used to quench $O_2^{\bullet-}$ since the addition of 1,4–benzoquinone would disturb the UV–vis analysis of RhB. During the reaction, the amount of added scavenger was 20 times greater than organic pollutant RhB. As shown in Fig. 14, in the presence of SOD, the RhB degradation was almost completely depressed, since the prevention of further H_2O_2 generation. Degradation studies using t–butanol as an $^\bullet$OH scavenger suggest that
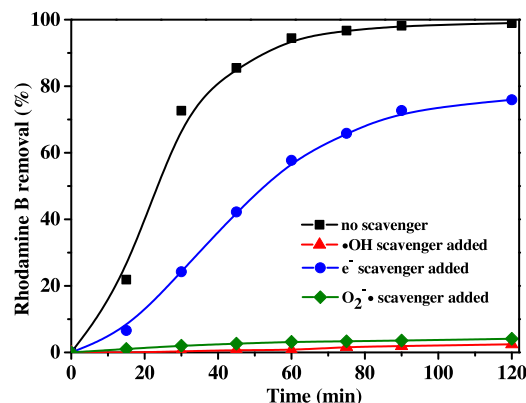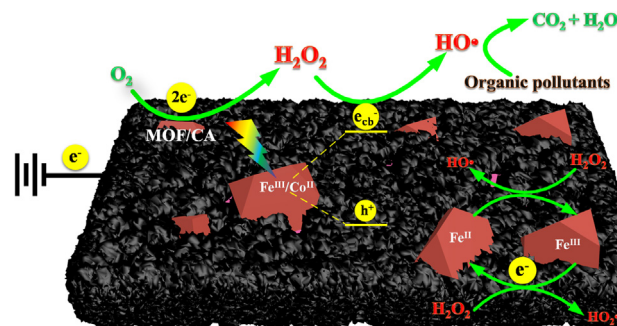

Fig. 15. Schematic illustration of solar–photo–electro–Fenton oxidation mechanism with MOF(2Fe/Co)/CA cathode in acidic condition.

$^\bullet$OH radicals are the sole dominant oxidant in the SPEF process for removing organic pollutants. With the addition of CCl_4 as e_{cb}^- scavenger, the RhB removal was decreased from 99% to 70%. Note that, after quenching e_{cb}^- with CCl_4, the RhB removal ($\sim$70% in Fig. 14) is still higher than in pure EF process with MOF(2Fe/Co)/CA cathode ($\sim$50% in Fig. 10A). This observation implied that Eq. (13) is still a competitive reaction with high reaction rate in the presence CCl_4. Overall, the collective results suggested that the photoinduced electron e_{cb}^- did significantly contribute to the improvement of $^\bullet$OH generation.

On the basis of the foregoing discussion, a reasonable schematic mechanism for enhancing the H_2O_2 and $^\bullet$OH generation with MOF(2Fe/Co)/CA cathode in SPEF process was illustrated in Fig. 15. Firstly, the two–electron reduction of adsorbed O_2 occurred with MOF(2Fe/Mo)/CA catalyst (Eq. (3)–(5)). The addition of MOF(2Fe/Co) behaves as the active sites for improving ORR activity and, hence, increases the yield of final product H_2O_2. Under visible–light irradiation, the electrons (e_{cb}^-) are excited from the valence band (VB) of MOF(2Fe/Co) and then enter into the conduction band (CB), leaving the holes (h^+) in the CB (Eq. (10)). Meanwhile, the photoinduced electron (e_{cb}^-) reacted with the electrogenerated H_2O_2 to form $^\bullet$OH radicals for effluents purification (Eq. (13)). Therefore, H_2O_2 behaving as electron acceptor can suppress the recombination of photoinduced eletron–hole pair, which is beneficial to the photocatalytic activity of MOF(2Fe/Co). The surface iron species (Fe^{III}) of MOF(2Fe/CA) would also interact with H_2O_2 according to the heterogeneous EF reaction mechanism[20]. The Fe^{III} active sites reacted with H_2O_2 to form $HO_2^\bullet$ oxidants and Fe^{II} sites through Eq. (17) [37]. Part of generated Fe^{II} sites further interacted with H_2O_2 to form $^\bullet$OH through Eq. (16). Interestingly, in heterogeneous EF process, a potential in–situ recycling of iron species ($Fe^{III} \rightarrow Fe^{II}$) would be easily occur on cathode through Eq. (17). That is why the main oxidants in EF process with
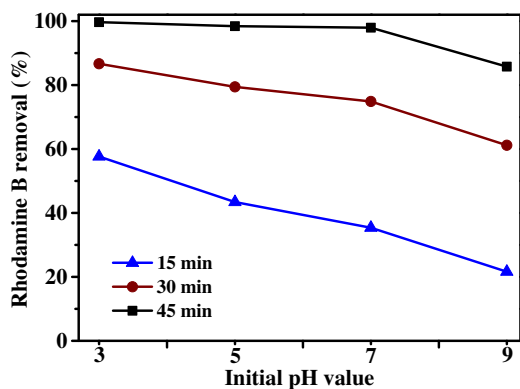
Fig. 16. The degradation efficiency of Rhodamine B with MOF(2Fe/Co)/CA cathode in SPEF process at different initial pH.
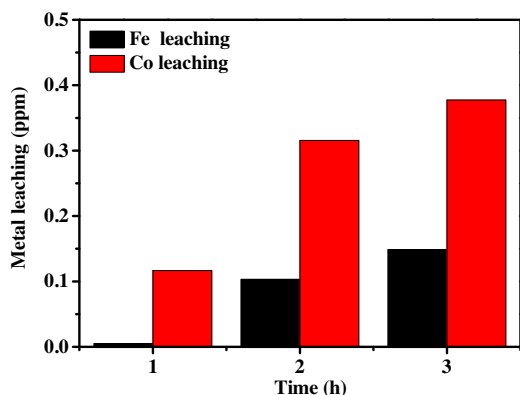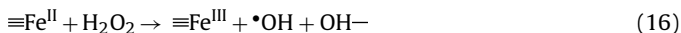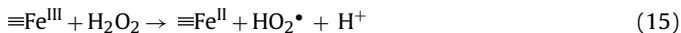

Fig. 17. Iron and cobalt leaching during the RhB degradation in the SPEF process.

MOF(2Fe/Co)/CA cathode was still •OH radicals, which is agreement with the EPR results as presented in Fig. 13.

$$\equiv Fe^{III} + H_2O_2 \rightarrow\ \equiv Fe^{II} + HO_2{}^\bullet + H^+ \tag{15}$$

$$\equiv Fe^{II} + H_2O_2 \rightarrow\ \equiv Fe^{III} + {}^\bullet OH + OH- \tag{16}$$

$$\equiv Fe^{III} + e^- \rightarrow\ \equiv Fe^{II} \tag{17}$$

So, in this SPEF reaction, high yield of H_2O_2 was obtained through two–electron reduction of O_2 with CA epically after the introduction of MOF(2Fe/Co). Once H_2O_2 was generated, the •OH radicals were continuously generated by photoinduced electron and surface iron species of MOF(2Fe/Co). And then the formed •OH radicals interacted with organic pollutants in terms of the surface adsorbed and solution dissolved, leading to final mineralization products.

3.5. The influence of operative pH condition and chemical stability of MOF(2Fe/Co)/CA in SPEF for wastewater treatment

The effect of initial pH on the catalytic oxidation ability of MOF(2Fe/Co)/CA in SPEF reaction was evaluated and shown in Fig. 16. At begin of degradation reaction (15 min), the increase of pH from 3 to 9 decreased the RhB degradation efficiency from 58% to 22%. Nevertheless, with increasing the reaction time, the pH variation had become little impact on RhB removal efficiency. For example, at 45 min, the RhB removal was 100%, 98%, 97%, 86% at pH = 3, 5, 7, and 9, respectively. This is possiblely due to that the electro–generate H_2O_2 by O_2 reduction on cathode $(O_2 + 2H^+ + 2e^- \rightarrow H_2O_2)$ was restrained with increasing pH especially at beginning of reaction. When increased reaction time is accompanied by the accumulation of H_2O_2, the effect of pH
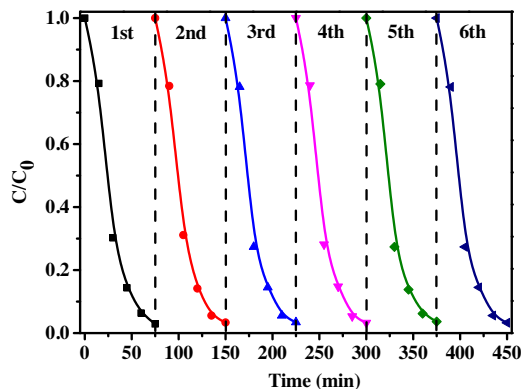

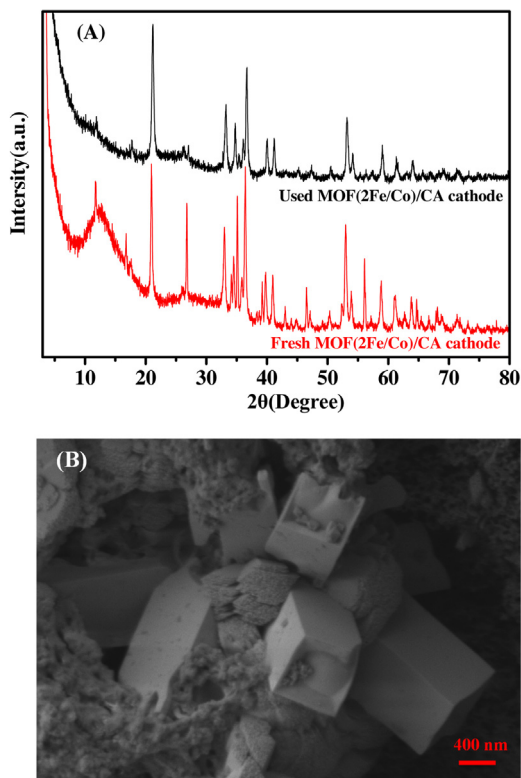**Fig. 18.** The stability of MOF(2Fe/Co)/CA cathode in the SPEF process.

Fig. 19. The XRD patterns of fresh and used MOF(2Fe/Co)/CA cathode, which had been reacted in SPEF process for 120 min at pH = 3 (A), and the SEM images of used MOF(2Fe/Co)/CA cathode (B).

on degradation efficiency becomes weak. These results further demonstrate that the catalytic activity of this EF reaction, mainly caused by photoinduced electrons of MOF(2Fe/Co), is quite stable within wide pH range without sacrificing efficiency.

From the perspective of actual application, the stability of cathode is an important issue that should be considered [15]. The leached iron and cobalt (C_{Fe} and C_{Co}) were monitored during SPEF reaction, as shown in Fig. 17. Both C_{Fe} and C_{Co} continuously increased with increasing the degradation time. Whereas, the C_{Fe} and C_{Co} were respectively only 0.15 and 0.37 ppm after 3 h, which is acceptable to the direct discharge stands (<1 ppm) in China. That is to say, the treated contaminates can be directly discharged into the sewage system after the SPEF process. The reusability is another key issue for evaluating the stability of catalysts. Thus, the recycling capacity of MOF(2Fe/Co)/CA was successfully carried out by degrading RhB over the reused cathode. As shown in Fig. 18, the degradation efficiency was nearly maintained at

the level of fresh sample after six consecutive runs. The obtained results greatly suggested that this novel fabricated MOF(2Fe/Co)/CA cathode exhibited good stability, which has a great potential for practical treatment of wastewater.

To determine the structural stability of MOF(2Fe/Co)/CA cathode, the morphology and crystal structure of the used cathode after SPEF reaction were examined by XRD and SEM. As shown in Fig. 19A, the main diffraction peaks of crystal were almost unchanged after interaction with H_2O_2 even in acidic solution. Moreover, the rectangular structure of MOF and porous of CA was remained the same as fresh sample (see Fig. 19B). All of these observations suggested the good stability of MOF(2Fe/Co)/CA cathode in SPEF process at pH = 3, which not only environmentally friendly but also economically viable.

4. Conclusions

The heterogeneous SPEF technology with bifunctional MOF(2Fe/Co)/CA as cathode has been investigated for the destruction of the azo-dye Rhodamine B (RhB) and endocrine disrupting dimethyl phthalate (DMP) as model pollutants. The optimal nFe:nCo ratio was 2:1 for MOF(2Fe/Co) to successfully grow on the surface of CA. A specific interaction affinity of FeOOH was obtained on MOF(2Fe/Co)/CA cathode. MOF(2Fe/Co) possessed bifunctional catalytic activities in terms of photocatalysis and electrocatalysis, while CA was served for H_2O_2 synthesis via the 2–electron pathway of ORR. The electron transfer number (n) of ORR process with CA was 2.5 in the selected potential range. The introduction of MOF(2Fe/Co) restrained the two–electron pathway but promoted the whole ORR activity, which finally improved the yield of H_2O_2. Meanwhile, the photoinduced electron (e_{cb}^-) of MOF(2Fe/Co) efficiently in–situ reacted with H_2O_2 for improving the generation of $^\bullet OH$ radicals. e_{cb}^- was an efficient and pH-independent Fenton-like catalysts. The degradation of RhB and DMP exhibited high catalytic oxidation performance. Almost 100% RhB removal and 85% DMP removal were reached in 45 min and 120 min at acidic media, respectively. The efficient degradation efficiency retained well in wide pH rage of 3–9. EPR and radical trapping experiments revealed that, $O_2^{\bullet-}$ radicals is the key parameter in controlling the H_2O_2 generation, while photoinduced e_{cb}^- plays as dominant role for the formation of $^\bullet OH$. The MOF(Fe/Co)/CA possessed high chemical stability with very low iron and cobalt leaching (<0.5 ppm) even in acidic media, which is acceptable to the direct discharge standards (<1 ppm) in China. This study provides new insight for developing efficient, reusable and pH-independent EF cathodes especially for enhancing on-site H_2O_2 and $^\bullet OH$ generation that can potentially be used for wastewater purification.

Acknowledgements

References

[1] L. Bounab, O. Iglesias, M. Pazos, M.Á. Sanromán, E. González-Romero, Appl. Catal. B: Environ. 180 (2016) 544–550.
[2] F. Sopaj, N. Oturan, J. Pinson, F. Podvorica, M.A. Oturan, Appl. Catal. B: Environ. 199 (2016) 331–341.
[3] C. Trellu, Y. Péchaud, N. Oturan, E. Mousset, D. Huguenot, E.D. van Hullebusch, G. Esposito, M.A. Oturan, Appl. Catal. B: Environ. 194 (2016) 32–41.
[4] Y. Wang, Y. Liu, T. Liu, S. Song, X. Gui, H. Liu, P. Tsiakaras, Appl. Catal. B: Environ. 156–157 (2014) 1–7.
[5] W.R.P. Barros, J.R. Steter, M.R.V. Lanza, A.C. Tavares, Appl. Catal. B: Environ. 180 (2016) 434–441.
[6] D. Farrusseng, S. Aguado, C. Pinel, Angew. Chem. Int. Ed. 48 (2009) 7502–7513.
[7] M.A. Nasalevich, M. van der Veen, F. Kapteijn, J. Gascon, CrystEngComm 16 (2014) 4919–4926.
[8] N.A. Khan, Z. Hasan, S.H. Jhung, J. Hazard. Mater. 244 (2013) 444–456.
[9] Z. Hasan, S.H. Jhung, J. Hazard. Mater. 283 (2015) 329–339.
[10] S.H. Huo, X.P. Yan, J. Mater. Chem. 22 (2012) 7449–7455.
[11] H. Lv, H. Zhao, T. Cao, L. Qian, Y. Wang, G. Zhao, J. Mol. Catal. A: Chem. 400 (2015) 81–89.
[12] A. Morozan, F. Jaouen, Energy Environ. Sci. 5 (2012) 9269–9290.
[13] H. Wang, F. Yin, G. Li, B. Chen, Z. Wang, Int. J. Hydrogen Energy 39 (2014) 16179–16186.
[14] Y.J. Wang, H.Y. Zhao, S.N. Chai, Y.B. Wang, G.H. Zhao, D.M. Li, Chem. Eng. J. 223 (2013) 524–535.
[15] H. Zhao, L. Qian, X. Guan, D. Wu, G. Zhao, Environ. Sci. Technol. 50 (2016) 5225–5233.
[16] C.H. Choi, H.C. Kwon, S. Yook, H. Shin, H. Kim, M. Choi, J. Phys. Chem. C 118 (2014) 30063–30070.
[17] Y. Liu, X. Quan, X. Fan, H. Wang, S. Chen, Angew. Chem. Int. Ed. 54 (2015) 6837–6841.
[18] C.H. Zhang, L.H. Ai, J. Jiang, J. Mater. Chem. A 3 (2015) 3074–3081.
[19] J.L. Wang, C. Wang, W.B. Lin, ACS Catal. 2 (2012) 2630–2640.
[20] H.Y. Zhao, Y.J. Wang, Y.B. Wang, T.C. Cao, G.H. Zhao, Appl. Catal. B: Environ. 125 (2012) 120–127.
[21] Q. Peng, H. Zhao, L. Qian, Y. Wang, G. Zhao, Appl. Catal. B: Environ. 174–175 (2015) 157–166.
[22] Y. Wang, H. Zhao, G. Zhao, Appl. Catal. B: Environ. 164 (2015) 396–406.
[23] J.Y. Feng, X.J. Hu, P.L. Yue, Environ. Sci. Technol. 38 (2004) 5773–5778.
[24] S.Q. Xie, J.Y. Hwang, X. Sun, S.Z. Shi, Z. Zhang, Z.W. Peng, Y.C. Zhai, J. Power Sources 253 (2014) 132–137.
[25] M.R. Lohe, M. Rose, S. Kaskel, Chem. Commun. (Camb.) (2009) 6056–6058.
[26] J. Ma, A. Habrioux, N. Guignard, N. Alonso-Vante, J. Phys. Chem. C 116 (2012) 21788–21794.
[27] J. Beltran-Huarac, O. Resto, J. Carpena-Nunez, W.M. Jadwisienczak, L.F. Fonseca, B.R. Weiner, G. Morell, ACS Appl. Mater. Interfaces 6 (2014) 1180–1186.
[28] L. Xu, X. Yang, Y. Guo, F. Ma, Y. Guo, X. Yuan, M. Huo, J. Hazard. Mater. 178 (2010) 1070–1077.
[29] Y. Nie, C. Hu, J. Qu, X. Zhao, Appl. Catal. B: Environ. 87 (2009) 30–36.
[30] Y. Hou, J. Qu, X. Zhao, H. Liu, J. Environ. Sci. 21 (2009) 1321–1328.
[31] F.L. Souza, J.M. Aquino, K. Irikura, D.W. Miwa, M.A. Rodrigo, A.J. Motheo, Chemosphere 109 (2014) 187–194.
[32] H.A. Hansen, V. Viswanathan, J.K. Nørskov, J. Phys. Chem. C 118 (2014) 6706–6718.
[33] L. Dai, Y. Xue, L. Qu, H.J. Choi, J.B. Baek, Chem. Rev. 115 (2015) 4823–4892.
[34] C.C. Wang, J.R. Li, X.L. Lv, Y.Q. Zhang, G. Guo, Energy Environ. Sci. 7 (2014) 2831–2867.
[35] J. He, J. Wang, Y. Chen, J. Zhang, D. Duan, Y. Wang, Z. Yan, Chem. Commun. (Camb.) 50 (2014) 7063–7066.
[36] M. Li, Z. Qiang, C. Pulgarin, J. Kiwi, Appl. Catal. B: Environ. 187 (2016) 83–89.
[37] A.L. Pham, F.M. Doyle, D.L. Sedlak, Environ. Sci. Technol. 46 (2012) 1055–1062.